Sensors & Actuators: B. Chemical 281 (2019) 415–423

Contents lists available at ScienceDirect

Sensors and Actuators B: Chemical

journal homepage: www.elsevier.com/locate/snb

One step synthesis of branched SnO_2/ZnO heterostructures and their enhanced gas-sensing properties

Xueli Yang, Sufang Zhang, Qi yu, Liupeng Zhao, Peng Sun*, Tianshuang Wang, Fangmeng Liu, Xu Yan, Yuan Gao, Xishuang Liang, Sumei Zhang, Geyu Lu*

State Key Laboratory on Integrated Optoelectronics, Key Laboratory of gas sensors, Jilin Province, College of Electronic Science and Engineering, Jilin University, 2699 Qianjin Street, Changchun 130012, China

ARTICLE INFO

Keywords:
SnO_2/ZnO
Hydrothermal method
Heterostructure
Gas sensor

ABSTRACT

In this work, a novel branched heterostructural composite composed of nanorods ZnO backbone and SnO_2 branches was prepared via a facile one-step hydrothermal method. The morphology, structure and component of the SnO_2/ZnO composite was characterized by field emission scanning electron microscopy (FESEM), transmission electron microscopy (TEM), X-ray powder diffraction (XRD), and elemental mapping analysis. The evolution process of the SnO_2/ZnO composite was observed by SEM that the SnO_2 branches gradually grow on ZnO backbones. The composite with novel heterostructure was applied as the sensing material for the fabrication of gas sensor, and their gas sensing properties were tested for response to various gases. Compared to pure ZnO gas sensors the branched SnO_2/ZnO gas sensor exhibited enhanced gas sensing properties toward ethanol, giving a response of 18.1–100 ppm.

1. Introduction

Metal oxide semiconductor gas sensors have been investigated extensively in recent years and used as a dominant and effective approach in the environment monitoring, air quality control, detection of inflammable, explosive, or toxic gases [1–4]. Thus, in recent years, a variety of semiconducting metal oxides such as SnO_2 [5,6], ZnO [7–9], WO_3 [10,11], In_2O_3 [12–14] and NiO [15–17] with various morphologies and microstructures have been investigated intensively for gas sensor applications to detect different test gases, including reducing gases and oxidizing gases [18–22]. Despite of exciting results have been obtained, the development of more highly sensitive and markedly selective gas sensors based on metal oxide semiconductors with novel nanostructures still remains a challenge. It has been demonstrated that the sensing properties of the semiconducting metal oxides are closely related to their composition, morphology, and crystalline size. So many approaches have been used to improve the sensitivity and selectivity of these oxides, including the loading of noble metal catalysts [23,24], the doping of transition metal ions [25,26], developing binary or ternary metal oxides [27]. Recently, many studies have confirmed that sensing materials constructing of two or more metal oxides show better sensing properties than that of a single metal oxide [28,29]. Therefore, many hybrid material such as α-Fe_2O_3/SnO_2 [30,31], SnO_2/ZnO [32–34], α-Fe_2O_3/ZnO [35,36], CeO_2/ZnO [37,38] and In_2O_3/ZnO [39,40] with different morphologies and structures have been investigated for gas sensing, and have achieved enhanced sensing property.

As important functional materials, ZnO and SnO_2 with band gaps of ~3.4 eV and ~3.6 eV, respectively, have been intensively investigated due to their unique properties and great potential applications such as gas sensors [41–43], solar cells [44,45], photocatalytic degradation [46,47] and lithium batteries [48,49]. Recently, many studies have demonstrated that the performance of ZnO or SnO_2 in gas sensing, photocatalytic degradation and lithium ion batteries can be significantly improved by formation of SnO_2/ZnO composites. Therefore, various SnO_2/ZnO composites with hierarchical microstructures have been prepared using different methods. However, to the best of our knowledge, studies of SnO_2/ZnO heterostructures obtained by a simple one-step hydrothermal route have been rarely reported.

In this work, SnO_2/ZnO heterostructures were successfully synthesized through a facile one-step hydrothermal method. The diameter of the as prepared ZnO backbone and SnO_2 branches were about 100 and 10 nm, respectively. The products were applied to fabricate gas sensing devices, and their gas sensing characteristics were systematically investigated. The results showed that, the SnO_2/ZnO heterostructures exhibited enhanced gas sensing properties toward ethanol compared with pure ZnO nanorods. The enhancement in sensing properties maybe

* Corresponding authors.
E-mail addresses: pengsun@jlu.edu.cn (P. Sun), lugy@jlu.edu.cn (G. Lu).

https://doi.org/10.1016/j.snb.2018.10.138
Received 2 May 2018; Received in revised form 14 September 2018; Accepted 26 October 2018
Available online 30 October 2018

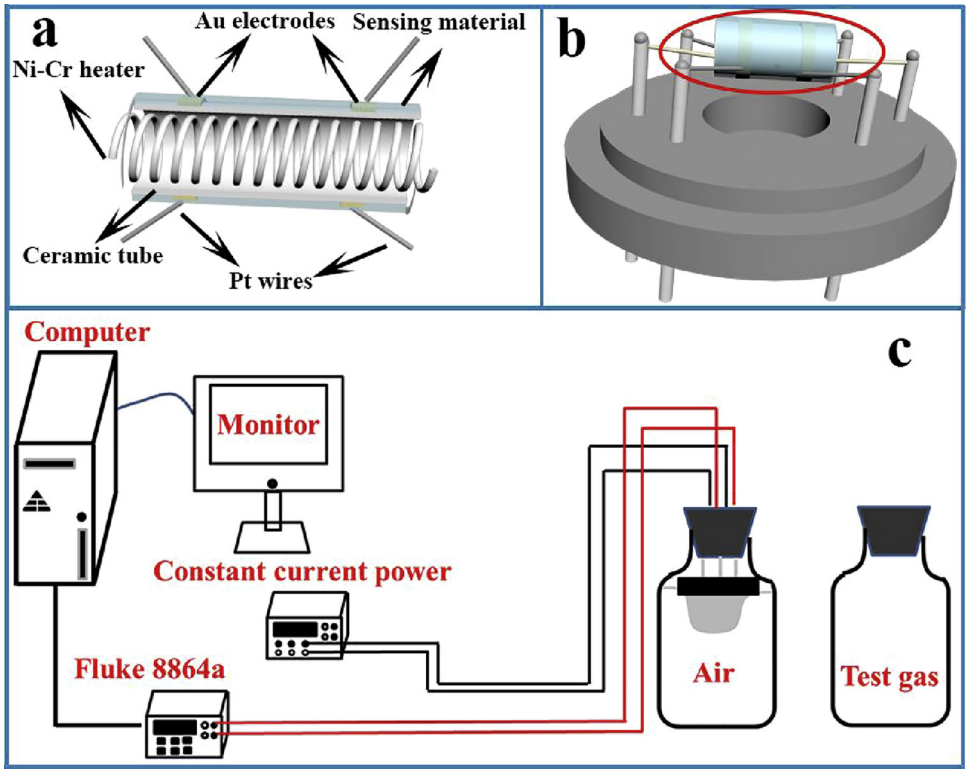

Fig. 1. Schematic diagram (a and b) and testing system (c) of the sensor.

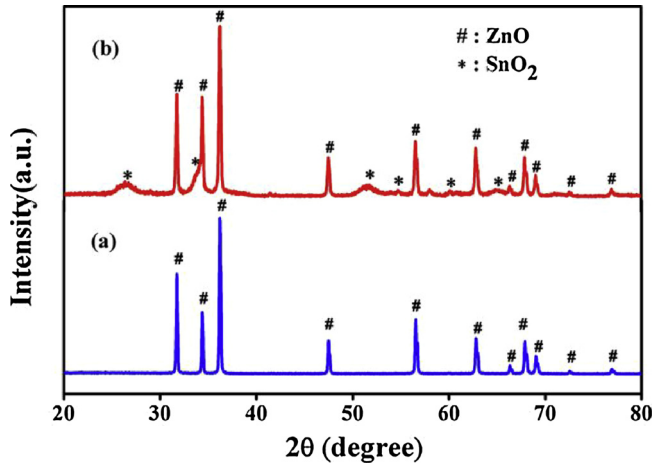

Fig. 2. XRD patterns of (a) the ZnO nanorods and (b) the SnO_2/ZnO composites.

attributed to the novel structure and the formation of SnO_2/ZnO heterojunction.

2. Experimental

2.1. Synthesis of SnO_2/ZnO composites

All of the reagents in the experiment were of analytical grade and used as received without further purification. The composites were prepared via a hydrothermal method. In a typical experiment, 1 mmol of zinc sulfate heptahydrate ($ZnSO_4{\cdot}7H_2O$) and 0.5 mmol of tin chloride pentahydrate ($SnCl_4{\cdot}5H_2O$) were dissolved in 40 mL of deionized water, after magnetic stirring for about 20 min, 15 mmol of NaOH were added into the above mixed solution and continued stirring for about 20 min, then the homogeneous solution was transferred into a 50 mL Teflon-lined stainless steel autoclave that was then sealed, maintained at 200 °C for 24 h. Subsequently the autoclave was allowed to cool down to room temperature naturally. The resulting precipitates were collected by centrifugation and washed several times with deionized water and ethanol alternately, then dried in air at 80 °C for 12 h. Finally, the SnO_2/ZnO branched nanostructure was obtained after annealing at 500 °C for 2 h in air atmosphere with a heating rate of 2 °C /min. For the preparation of rod-like ZnO, all the steps were remain unchanged except for the addition of $SnCl_4{\cdot}5H_2O$.

2.2. Characterization

The crystal structure of the obtained products were characterized by X-ray diffractometer (XRD, Rigaku D/Max-2550 V, Cu-Kα radiation. λ = 1.54178 Å). The morphology and microstructure of the product was observed by field emission scanning electron microscopy (FESEM) on a JSM-7500 F (JEOL) microscope operating at an accelerating voltage of 15 kV. Transmission electron microscopy (TEM) and high-resolution transmission electron microscopy (HRTEM), and selected area electron diffractive (SAED) patterns were carried out on a JEM-2200FS apparatus (JEOL) operating at 200 kV. The energy dispersive X-ray spectrometry (EDS) result was measured by the TEM attachment. The surface elemental composition was performed with X-ray photoelectron spectroscopy (XPS, Thermo ESCALAB 250XI). All of the binding energies in the XPS analysis were calibrated for specimen charging by reflecting to the signal of carbon C 1s peak with a binding energy of 284.7 eV.

2.3. Fabrication and gas sensing measurements

The fabrication of gas sensors and gas sensing measurements were described as follows: the as-prepared products were mixed with deionized water to form a slurry, and then coated on the ceramic tube (4 mm in length, 1.2 mm in external diameter, and 0.8 mm in internal diameter, attached with a pair of gold electrodes) by a small brush to form a thick film. After drying in air at room temperature, the device

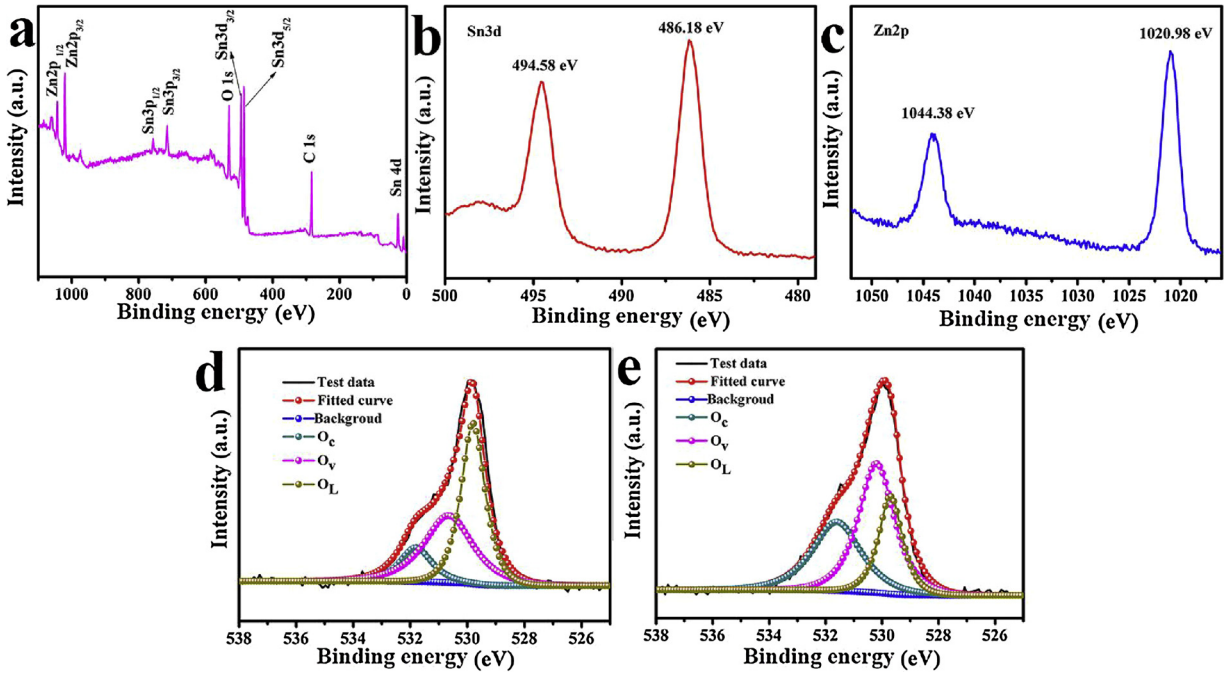

Fig. 3. XPS spectra and the fitted data of (a) Full survey scan XPS spectra of branched SnO_2/ZnO, (b) Sn 3d, (c) Zn 2p, (d) O 1s of the pure ZnO rods, and (e) O 1s spectrum of branched SnO_2/ZnO composites.

Table 1
Fitting Results of O 1s XPS Spectra of pure ZnO and SnO_2/ZnO composites.

Sample	Oxygen Species	Binding Energy (eV)	Relative Percentage (%)
Pure ZnO	O_L(Zn-O)	529.8	47.4
	O_v(vacancy)	530.6	39.5
	O_c(chemisorbed)	531.8	13.0
SnO2/ZnO Composites	O_L(Zn-O)	529.7	22.7
	O_v(vacancy)	530.2	45.2
	O_c(chemisorbed)	531.6	32.1

was calcined at 400 °C for 2 h. The Ni-Cr alloy coil heater was inserted into the alumina tube to control the operating temperature by adjusting the heating current. The structure of the sensor is shown in Fig. 1a and b. The gas-sensing performance of the sensor was evaluated with a RG-2 gas sensing characterization system under laboratory conditions (30 RH %, 23 °C) as depicted in Fig. 1c. The gas sensing performance of the gas sensor was investigated using a static system. A given amount of the tested gas was injected into a closed glass chamber, and the sensor was put into the chamber for the measurement of the sensitive performance. The sensor response is defined as the ratio of R_a/R_g, where R_a and R_g are the resistances of the sensors in air and in target gas, respectively. The response (τ_{res}) and recovery time (τ_{recov}) is defined as the time taken by the sensor to achieve 90% of the total resistance change in the case of adsorption and desorption.

3. Results and discussion

3.1. Structural and morphological characteristics

The crystalline structure and the composition of the as obtained products were identified by means of XRD analysis. Fig. 2 displays the XRD patterns of the as-synthesized ZnO nanorods and the SnO_2/ZnO composites. Clearly, both of the two products revealed very sharp diffraction peaks due to their high crystallinity. All of the diffraction peaks in curve (a) were matched well with the hexagonal ZnO (JCPDS No. 89-1397). Compared with the XRD pattern of pure ZnO anorods, the newly emerged peaks illustrated in Fig. 2b were well indexed to tetragonal rutile structure of SnO_2 (JCPDS No. 41-1445). It is obvious that no other impurities were observed which confirmed the final product to be a composite of ZnO and SnO_2.

X-Ray photoelectron spectroscopy (XPS) analysis was also performed to analyze the surface chemical composition and chemical state of the ZnO and SnO_2/ZnO composites. Fig. 3a shows the full range spectrum of SnO_2/ZnO composites, it could be seen that all the peaks corresponded to Sn, Zn, O and C, no other impurities could be observed, confirming the high purity of the obtained materials. Fig. 3b displays the XPS spectra of Sn. Two peaks with binding energies at 486.18 eV and 494.58 eV could be attributed to the bonding energies of Sn $3d_{5/2}$ and $3d_{3/2}$, respectively, which were characteristic of Sn^{4+} cations [49]. The bonding energies at 1020.98 eV and 1044.38 eV corresponded to the Zn $2p_{3/2}$ and Zn $2p_{1/2}$ (Fig. 3c), respectively, indicating the existing of Zn^{2+} [50] in the composites. Fig. 3d and e exhibits the O 1s XPS spectra of the pure ZnO and SnO_2/ZnO composites. It can be found that both of the tested curves could be decomposed into three significant oxygen species [51].The lattice oxygen species expressed with O_L, the oxygen vacancy species component was represented with O_V, and the chemisorbed oxygen species component signified as O_C. Table 1 lists all the center positions and the relative percentages of each oxygen species component peak. The O_v component amount of the two samples almost had no change. However, it is obvious that the relative percentage of O_C component of SnO_2/ZnO composites (32.1%) increased a lot comparing with pure ZnO rods (13.0%), which was much higher than ZnO rods. Thus, the surface oxygen absorbed ability was greatly improved, which enhanced the capable of reacting with test gas molecules, leading to good gas sensing performance as sensing material.

The surface morphology and microstructure of the products were investigated by SEM and TEM observations. Fig. 4 shows typical SEM images of the as-prepared ZnO rods and SnO_2/ZnO branched nanostructures. It can be seen that the ZnO rods had uniform morphology and smooth surface (Fig. 4a and b), and some of the rods stuck together. The diameter of the ZnO rods was about 500 nm and the length of the rods was more than 5 μm as shown in the inset of Fig. 4b. The SEM image (Fig. 4c and d) of SnO_2/ZnO nanostructures shows that the as synthesized SnO_2/ZnO composites had branched morphology with ZnO as the

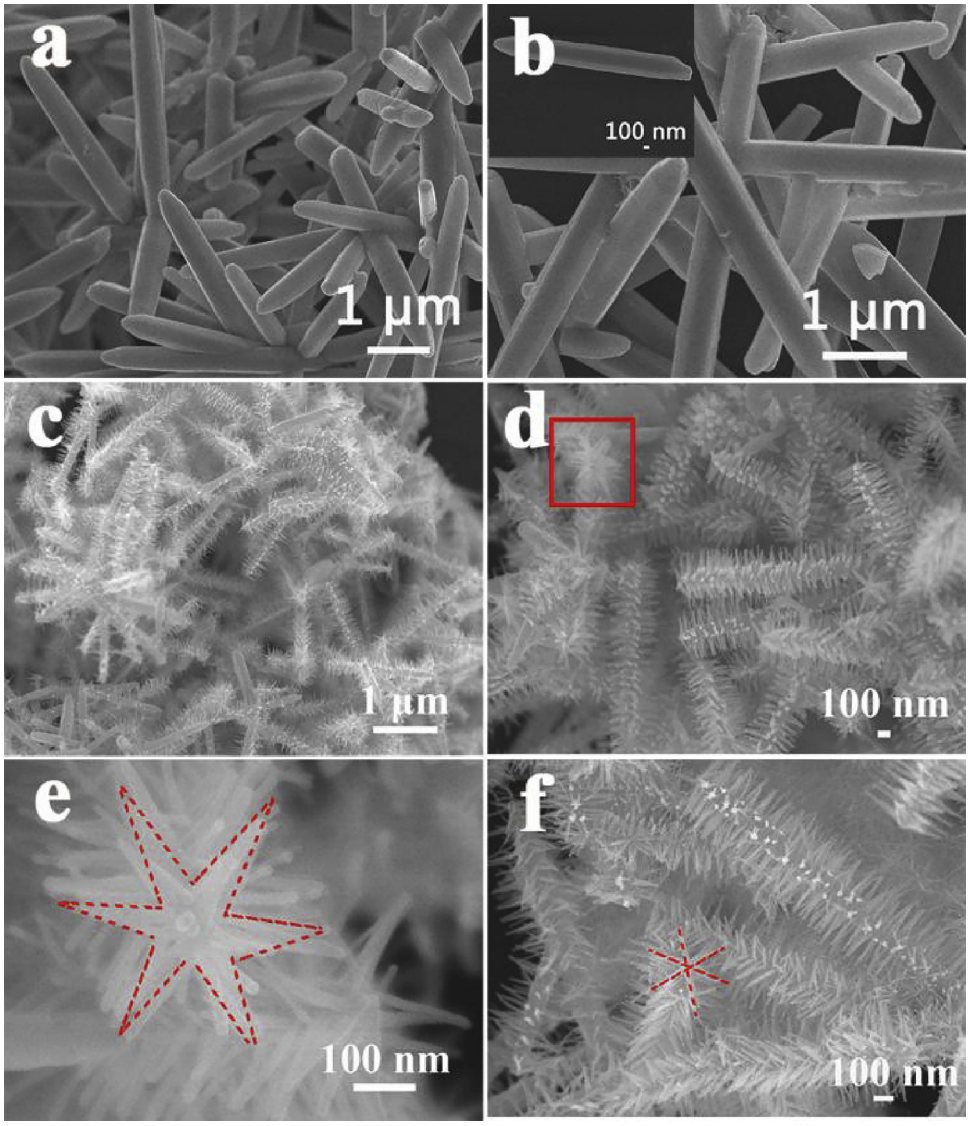

Fig. 4. SEM images of (a and b) pure ZnO and (c–f) SnO_2/ZnO composites. (For interpretation of the references to colour in the figure text, the reader is referred to the web version of this article.)

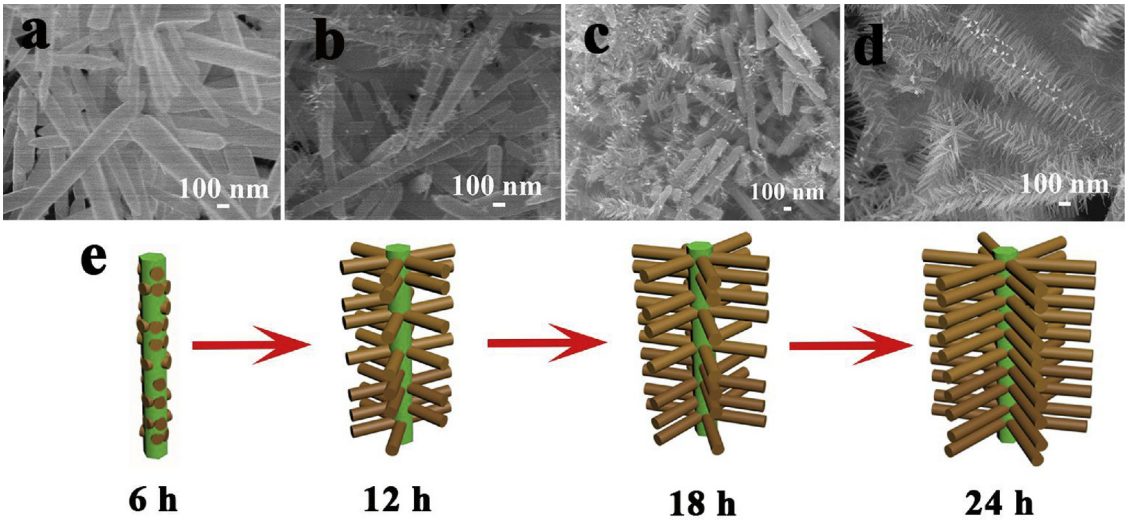

Fig. 5. SEM images of SnO_2/ZnO with different hydrothermal temperature (a) 6 h, (b) 12 h, (c) 18 h, (d) 24 h. (e) Schematic diagram of growing mechanism during hydrothermal process of branched SnO_2/ZnO composites.

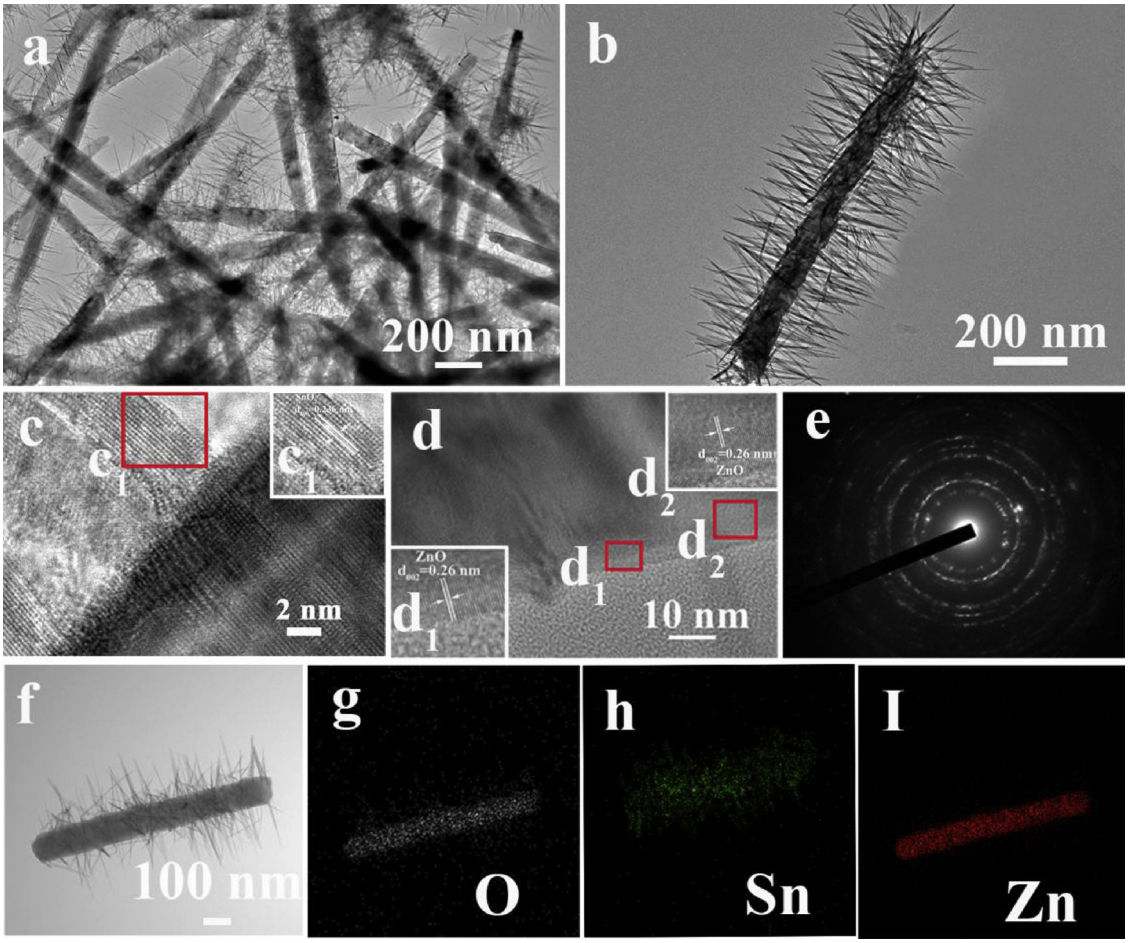

Fig. 6. (a) Low magnification and (b) high magnification transmission electron microscopy (TEM) images of SnO_2/ZnO composites. (c and d) HRTEM images of SnO_2/ZnO composites. (e) SAED patterns of the SnO_2/ZnO composites. (f–i) TEM image of an individual SnO_2/ZnO nanostructure and the corresponding elemental mapping images.

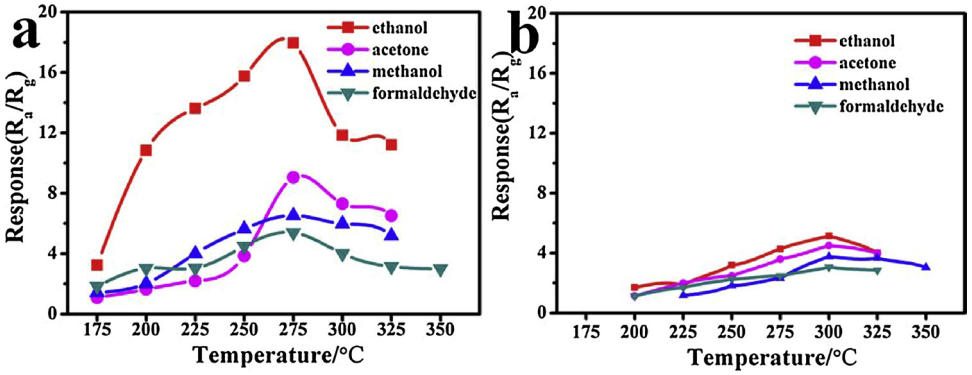

Fig. 7. (a) Response of SnO_2/ZnO composites and (b) pure ZnO rods upon exposed to 100 ppm ethanol, acetone, methanol, formaldehyde as a function of operating temperature.

backbones and SnO_2 as the branches. Fig. 4d shows that the diameter of the ZnO was approximately 100 nm which was much thinner than that of pure ZnO rods (Fig. 4b). It can be seen from the enlarged marked red rectangle of Fig. 4d in Fig. 4e, the SnO_2 branches with 20 nm in diameter were uniformly grown on the ZnO nanorods and formed a six symmetrical branched structure. Fig. 4f also demonstrated that the SnO_2 branches formed a six symmetrical structure.

In order to investigate the evolution process of the SnO_2/ZnO nanostructure, time-dependent evolution hydrothermal processes with different hydrothermal time of 6, 12, 18 and 24 h were carried out, as shown in Fig. 5. It can be seen that the ZnO and SnO_2 were grown simultaneously under the hydrothermal condition. Fig. 5a shows the SEM image of the composites after reaction for 6 h, the products were almost ZnO nanorods. With the reaction time extended to 12 h, some SnO_2 branches appeared on the ZnO backbones and the length of the SnO_2 branches grew with the reaction time (as seen from Fig. 5c). While the reaction time extended to 24 h, it can be seen in Fig. 5d that the SnO_2 branches were uniformly grown on the ZnO nanorods. The XRD patterns of the corresponding SnO_2/ZnO composites with different reaction time are depicted in Fig. S1. On the basis of the results stated

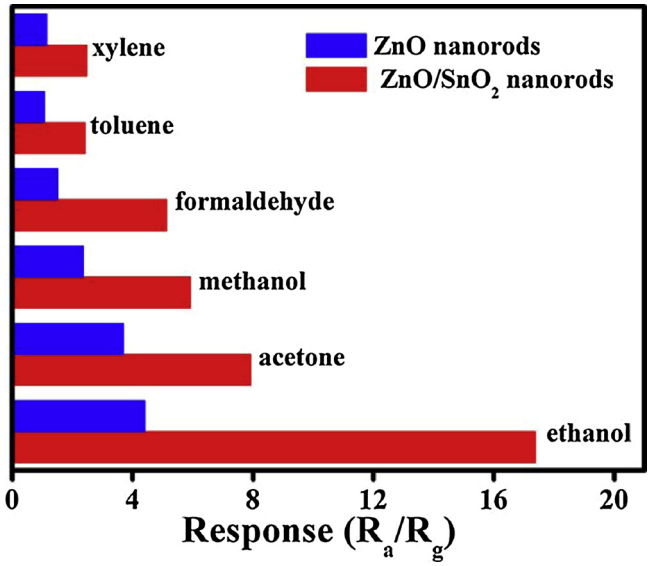

Fig. 8. Selectivity measurements of the pure ZnO and SnO_2/ZnO composites to various test gases with concentrations of 100 ppm.

Table 2
Comparison of different ethanol gas sensors based on SnO_2, ZnO and SnO_2/ZnO.

Sensing material	Morphology	Tem. (°C)	Con. (ppm)	Res. (Ra/Rg)	Ref.
SnO_2	nanospheres	300	100	9.2	[52]
SnO_2	Ordinary nanofiber	250	100	7.6	[53]
ZnO	nanoflowers	340	50	3.9	[54]
ZnO	nanowire	340	500	10.68	[55]
ZnO	flower-like	300	100	13.2	[56]
SnO_2/ZnO	nanosheets	350	100	13.3	[57]
SnO_2/ZnO	nanorods	275	100	18.1	This work

above, the formation process of the SnO_2/ZnO composites during the hydrothermal process was proposed, as schematically illustrated in Fig. 5e.

TEM and HRTEM measurements were carried out in order to get deeper insight into the structure of the SnO_2/ZnO composites. Fig. 6a and b shows the typical images of the SnO_2/ZnO composites, it can be seen in Fig. 6a that the as-synthesized composites have uniform morphology, SnO_2 branches grew on the ZnO backbones. Fig. 6b displays the high magnification morphology of the products. It is found that the diameter and length of the ZnO backbones was about 100 nm and 1 μm, respectively. The SnO_2 branches were thin and uniformly grew on the ZnO backbones. The diameter of SnO_2 branches was nearly 20 nm, while the length of the SnO_2 was no more than 500 nm. The TEM images are matched well with the SEM observation. HRTEM was carried out to further study the detailed lattice structure. The HRTEM images of the branches marked with red rectangles in Fig. 6c indicate the lattice fringe spacing of 0.33 nm corresponding to the (110) lattice plane of SnO_2. Fig. 6d shows the HRTEM images of the SnO_2/ZnO backbones. The lattice fringe spacing of 0.26 nm in the two inset images corresponded to the (002) lattice plane of ZnO. Fig. 6e displays the selected area electron diffraction (SAED) patterns of the SnO_2/ZnO composites and the result indicates that the SnO_2/ZnO composites were polycrystalline. In addition, the TEM image and elemental mapping of a single SnO_2/ZnO nanostructure are displayed in Fig. 6f–i. It can be seen that the O and Sn were distributed on both the backbones and branches, while Zn was only distributed on the backbones. This result agreed well with the HRTEM images.

3.2. Gas sensing characteristics

The gas sensing properties of the SnO_2/ZnO hierarchical structure and bare ZnO rods to different test gas were measured. Fig. 7a and b display the response of the two sensors to 100 ppm ethanol, acetone, methanol and formaldehyde at operating temperature from 175 to 350 °C. It is found that the response of the sensors to different test gas varied with the temperature, and increased with a raise of operating temperature, and reached the maximum value, then decreased with further increasing temperature. The sensor based on SnO_2/ZnO reached the maximum value of 18.1 to 100 ppm ethanol at 275 °C, while the maximum value reached 4.5 at 300 °C for the sensor based on pure ZnO. Apparently, the sensor based on the SnO_2/ZnO possessed a relatively low operating temperature and enhanced sensing response.

Since selectivity is an important parameter to evaluate the sensing performances of gas sensor. Thus, the selectivity of the two sensors was investigated by exposed to various test gases with a concentration of 100 ppm at the operating of 275 °C and 300 °C, respectively, as shown in Fig. 8. Obviously the two sensors exhibited much higher response to ethanol than that of other tested gases, indicating the good selectivity for ethanol. In addition, it is worth noting that the sensing properties of SnO_2/ZnO composites were greatly improved compared to pure ZnO sensor, such as the response to ethanol was as 3-fold as high as the pure ZnO. The sensing performance comparison between pure SnO_2, ZnO and SnO_2/ZnO ethanol sensor in reported literature and our present work was made. As illustrated in Table 2 [52–57], apparently, compared with pure SnO_2 and ZnO based sensors, the branched SnO_2/ZnO heterostructures exhibited much higher response at a relatively lower operating temperature than the others.

Fig. 9a displays the sensing behaviors of the two sensors to ethanol

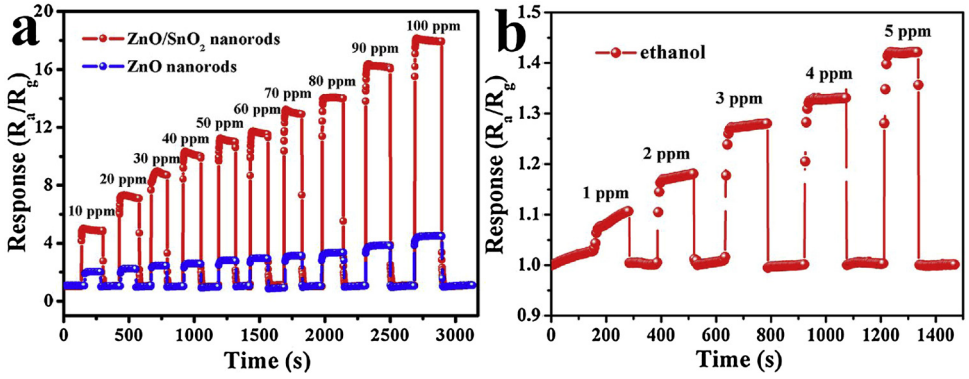

Fig. 9. (a) Dynamic response curves of pure ZnO and SnO_2/ZnO composites to different concentrations of ethanol. (b) Dynamic response curves of SnO_2/ZnO composites to ethanol with a concentration of 1–5 ppm.

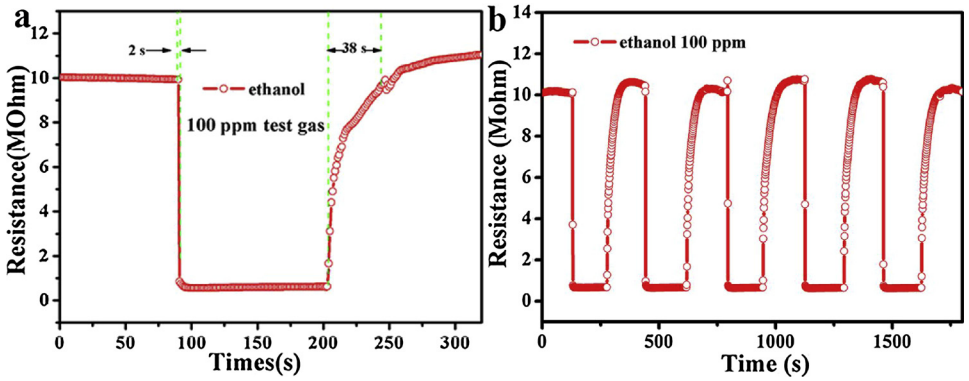

Fig. 10. (a) response transients of SnO_2/ZnO composites to ethanol with a concentration of 100 ppm at 275 °C. (b) Five periods of reponse-recovery curve to 100 ppm ethanol at the operating temperature of 275 °C.

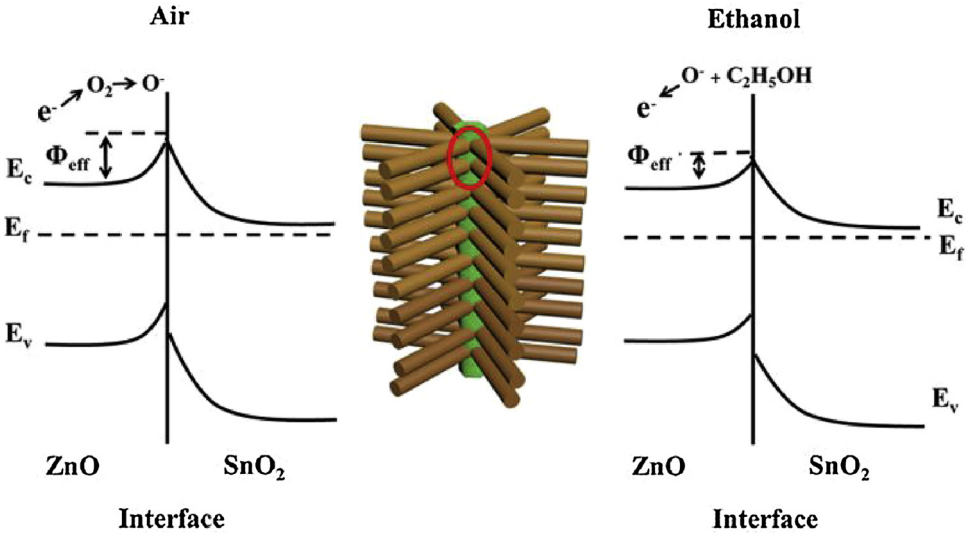

Fig. 11. Schematic diagrams of the energy band structure of the SnO_2/ZnO heterostructures in air and ethanol.

with the concentration range from 10 to 100 ppm at 275 °C and 300 °C, respectively. The gas responses of the two sensors present a stepwise distribution with the increasing of ethanol concentration. Obviously, the SnO_2/ZnO heterostructure exhibited higher response to ethanol than that of pure ZnO rods. The corresponding response values of SnO_2/ZnO heterostructure were 4.9, 7.3, 9.0, 10.3, 11.2, 11.6, 13.1, 14.2, 16.3 and 18.1, while for the pure ZnO, the response values were merely 2.0, 2.2, 2.4, 2.7, 2.8, 3.0, 3.1,3.3,3.8 and 4.5. Fig. 9b depicts the SnO_2/ZnO sensor to ethanol with a concentration of 1 to 5 ppm. The response was 1.0, 1.17, 1.27, 1.32 and 1.41, which indicated the sensor has a low detection limit.

Fig. 10a displays the dynamic response and recovery curves of SnO_2/ZnO to 100 ppm ethanol at 275 °C. It can be found that the resistance of sensor immediately changed when the sensor was exposed to tested gases, and then reached a steady state. The response time of the sensor to ethanol was within 3 s and the recovery time was 38 s. In addition, Fig. 10b shows the five cycles of the response and recovery curves of SnO_2/ZnO sensor to 100 ppm ethanol at 275 °C, indicating stable and repeatable characteristics of the sensor to ethanol.

3.3. Gas sensing mechanism

The basic sensing mechanism of n-type semiconductor sensors has been well documented with the space-charge layer model [58,59]. The conductivity of semiconductor will change when the gas sensor is exposed to different gases. This is the basic working principle of oxide semiconductor sensors. In ambient air, oxygen molecules can absorb on the surface of the sensing material and form surface absorbed oxygen species ($O_{2(ads)}^-$, $O_{(ads)}^-$ and $O_{(ads)}^{2-}$, Eqs. (1)–(4)) by capturing free electrons from their conducting bands. The reaction can be described as follows: [60]

$$O_2 \rightarrow O_{2\ (ads)} \quad (1)$$

$$O_{2\ (ads)} + e^- \rightarrow O_{2(ads)}^- \quad (2)$$

$$O_{2(ads)}^- + e^- \rightarrow 2O^-_{\ (ads)} \quad (3)$$

$$O^-_{\ (ads)} + e^- \rightarrow O_{(ads)}^{2-} \quad (4)$$

In this process, a thick electron depletion layer will be formed on the surface, resulting in a decrease of carrier concentration and an increase of sensor resistance. When the sensor is exposed to reducing gases at a moderate temperature, the absorbed oxygen species will react with these gas molecules. As a result, the electrons trapped in the oxygen species are released back into the conduction band, leading to the decrease of the thickness of depletion layer and the resistance of the sensor.

The gas sensing selectivity can be affected by many factors according to the literature, such as the LUMO (lowest unoccupied molecule orbit) energy of gas molecule and the amount of gas adsorption on the sensing material at different operating temperature. A lower LUMO energy will reduce the energy needed for gas sensing reaction. Moreover, the electron affinity is affected by the orbital energy of the gas molecule, if the value of LUMO energy is lower, the gas molecule ability in capturing electrons will be stronger. Therefore, at the

operating temperature of 275 °C, due to the LUMO energy of ethanol is lower than other test gases, the ability of capturing electrons of ethanol will be stronger than other test gases, and therefore the sensor will exhibit higher response to ethanol [61].

The above experimental results demonstrated that the SnO_2/ZnO heterostructure exhibited much better sensing performances than that of pure ZnO. The enhancement in sensing response of SnO_2/ZnO can be attributed to the following factors. First, the surface of ZnO backbones are not completely enclosed by SnO_2 branches, resulting in both of the two oxides being highly accessible for the adsorption of oxygen molecules and promoting the formation of depletion layers on the surface. Therefore, the synergetic effect of the two oxides maybe contributes to the enhancement of the sensing performance compared to the pure ZnO.

Secondly, the work functions of ZnO and SnO_2 have been reported to be 5.2 and 4.9 eV, respectively [62], which leads to the formation of heterojunction between ZnO and SnO_2. A proposed energy band structure diagram of the SnO_2/ZnO heterojunction is elucidated schematically in Fig. 11. The electrons will flow from SnO_2 to ZnO until their Fermi levels equalize. This process creates an electron depletion layer on the surface of SnO_2 and further bends the energy band and lead to a higher resistance state of the SnO_2/ZnO material. When the sensor exposes to reductive gas atmosphere at a moderate temperature, the trapped electrons are released back to the conduction band of SnO_2/ZnO material due to the reaction between these gas molecules and the absorbed oxygen species. Consequently, the conductivity of the heterostructures will be greatly increased, which results in high response.

4. Conclusion

In summary, the branched SnO_2/ZnO heterostructures composed of ZnO as backbones and SnO_2 as branches were successfully synthesized through a facile one-step hydrothermal method. The morphological and structural properties of the composites were characterized by various analysis techniques. The structure features of the composites at different reaction stages were investigated to explore the formation mechanism of such novel structure. Subsequently, the as-synthesized composites were fabricated gas sensor, and their sensing performances were evaluated. The results turned out that the SnO_2/ZnO composites exhibited excellent ethanol-sensing properties. The reason of performance improvement has been discussed. This is because the ZnO and SnO_2 formed N–N heterojunction which greatly increase the resistance of the sensor compared pure ZnO. This is the main reason for the enhanced response to ethanol. This study provides a rational way for the design and fabrication of the chemiresistive gas sensor with high performance.

Acknowledgements

This work is supported by the National Key Research and Development Program (No. 2016YFC0207300). National Nature Science Foundation of China (Nos. 61833006, 61722305, 61503148, 61520106003, 61327804). Science and Technology Development Program of Jilin Province (No. 20170520162JH). China Postdoctoral Science Foundation funded project Nos. 2017T100208 and 2015M580247. Program for JLU Science and Technology Innovative Research Team. Fundamental Research Funds for the Central Universities.

Appendix A. Supplementary data

Supplementary material related to this article can be found, in the online version, at doi:https://doi.org/10.1016/j.snb.2018.10.138.

References

[1] N. Yamazoe, Toward innovations of gas sensor technology, Sens. Actuators B Chem. 108 (2005) 2–14.
[2] G.F. Fine, L.M. Cavanagh, A. Afonja, R. Binions, Metal oxide semi-conductor gas sensors in environmental monitoring, Sensors 10 (2010) 5469–5502.
[3] Y. Cui, Q. Wei, H. Park, C.M. Lieber, Nanowire nanosensors for highly sensitive and selective detection of biological and chemical species, Science 293 (2001) 1289–1292.
[4] K. Wetchakun, T. Samerjai, N. Tamaekong, C. Liewhiran, C. Siriwong, V. Kruefu, A. Wisitsoraat, A. Tuantranont, S. Phanichphant, Semiconducting metal oxides as sensors for environmentally hazardous gases, Sens. Actuators B Chem. 160 (2011) 580–591.
[5] Y. Zou, S. Chen, J. Sun, J. Liu, Y. Che, X. Liu, J. Zhang, D. Yang, Highly efficient gas sensor using a hollow SnO_2 microfiber for triethylamine detection, ACS Sens. 2 (2017) 897–902.
[6] H. Wang, A.L. Rogach, Hierarchical SnO_2 nanostructures: recent advances in design, synthesis, and applications, Chem. Mater. 26 (2014) 123–133.
[7] T. Park, E.K. Kang, N.R. Kim, Y. Oh, J.K. Yoo, M.K. Um, Aspect ratio-controlled ZnO nanorods for highly sensitive wireless ultraviolet sensor applications, J. Mater. Chem. C 5 (2017).
[8] Z. Jing, J. Zhan, Fabrication and gas-sensing properties of porous ZnO nanoplates, Adv. Mater. 20 (2008) 4547–4551.
[9] J. Gonzalez-Chavarri, L. Parellada-Monreal, I. Castro-Hurtado, E. Castano, G.G. Mandayo, ZnO nanoneedles grown on chip for selective NO_2 detection indoors, Sens. Actuators B Chem. 255 (2018) 1244–1253.
[10] J. Ma, Y. Ren, X. Zhou, L. Liu, Y. Zhu, X. Cheng, P. Xu, X. Li, Y. Deng, D. Zhao, Pt nanoparticles sensitized ordered mesoporous WO_3 semiconductor: gas sensing performance and mechanism study, Adv. Funct. Mater. 28 (2018).
[11] S.S. Shendage, V.L. Patil, S.A. Vanalakar, S.P. Patil, N.S. Harale, J.L. Bhosale, J.H. Kim, P.S. Patil, Sensitive and selective NO_2 gas sensor based on WO_3 nanoplates, Sens. Actuators B Chem. 240 (2017) 426–433.
[12] M. Ding, N. Xie, C. Wang, X. Kou, H. Zhang, L. Guo, Y. Sun, X. Chuai, Y. Gao, F. Liu, P. Sun, G. Lu, Enhanced NO_2 gas sensing properties by Ag-doped hollow urchin-like In_2O_3 hierarchical nanostructures, Sens. Actuators B Chem. 252 (2017) 418–427.
[13] S. Zhang, P. Song, H. Yan, Q. Wang, Self-assembled hierarchical Au-loaded In_2O_3 hollow microspheres with superior ethanol sensing properties, Sens. Actuators B Chem. 231 (2016) 245–255.
[14] F. Gu, R. Nie, D. Han, Z. Wang, In_2O_3-graphene nanocomposite based gas sensor for selective detection of NO_2 at room temperature, Sens. Actuators B Chem. 219 (2015) 94–99.
[15] Y. Zhang, W. Zeng, New insight into gas sensing performance of nanoneedle-assembled and nanosheet-assembled hierarchical NiO nanoflowers, Mater. Lett. 195 (2017) 217–219.
[16] N.G. Cho, I.-S. Hwang, H.-G. Kim, J.-H. Lee, I.-D. Kim, Gas sensing properties of p-type hollow NiO hemispheres prepared by polymeric colloidal templating method, Sens. Actuators B Chem. 155 (2011) 366–371.
[17] G. Zhu, C. Xi, H. Xu, D. Zheng, Y. Liu, X. Xu, X. Shen, Hierarchical NiO hollow microspheres assembled from nanosheet-stacked nanoparticles and their application in a gas sensor, RSC Adv. 2 (2012) 4236–4241.
[18] X. Chen, C.K.Y. Wong, C.A. Yuan, G. Zhang, Nanowire-based gas sensors, Sens. Actuators B Chem. 177 (2013) 178–195.
[19] F.-T. Liu, S.-F. Gao, S.-K. Pei, S.-C. Tseng, C.-H.J. Liu, ZnO nanorod gas sensor for NO_2 detection, J. Taiwan Inst. Chem. Eng. 40 (2009) 528–532.
[20] J. Wang, X. Li, Y. Xia, S. Komarneni, H. Chen, J. Xu, L. Xiang, D. Xie, Hierarchical ZnO nanosheet-nanorod architectures for fabrication of poly(3-hexylthiophene)/ZnO hybrid NO_2 sensor, ACS Appl. Mater. Interfaces 8 (2016) 8600–8607.
[21] J. Li, X. Liu, J. Cui, J. Sun, Hydrothermal synthesis of self-assembled hierarchical tungsten oxides hollow spheres and their gas sensing properties, ACS Appl. Mater. Interfaces 7 (2015) 10108–10114.
[22] Y. Zhang, X. He, J. Li, H. Zhang, X. Gao, Gas-sensing properties of hollow and hierarchical copper oxide microspheres, Sens. Actuators B Chem. 128 (2007) 293–298.
[23] W.H. Tao, C.H. Tsai, H_2S sensing properties of noble metal doped WO_3 thin film sensor fabricated by micromachining, Sens. Actuators B Chem. 81 (2002) 237–247.
[24] M.V. Vaishampayan, R.G. Deshmukh, I.S. Mulla, Influence of Pd doping on morphology and LPG response of SnO_2, Sens. Actuators B Chem. 131 (2008) 665–672.
[25] X. Li, Y. Chang, Y. Long, Influence of Sn doping on ZnO sensing properties for ethanol and acetone, Mater. Sci. Eng. C-Mater. 32 (2012) 817–821.
[26] X. Kou, N. Xie, F. Chen, T. Wang, L. Guo, C. Wang, Q. Wang, J. Ma, Y. Sun, H. Zhang, G. Lu, Superior acetone gas sensor based on electrospun SnO_2 nanofibers by Rh doping, Sens. Actuators B Chem. 256 (2018) 861–869.
[27] H.M. Jeong, J.H. Kim, S.Y. Jeong, C.H. Kwak, J.H. Lee, Co_3O_4-SnO_2 hollow heteronanostructures: facile control of gas selectivity by compositional tuning of sensing materials via galvanic replacement, ACS Appl. Mater. Interfaces 8 (2016) 7877–7883.
[28] D.R. Miller, S.A. Akbar, P.A. Morris, Nanoscale metal oxide-based heterojunctions for gas sensing: a review, Sens. Actuators B Chem. 204 (2014) 250–272.
[29] F. Qu, Y. Wang, Y. Wang, J. Zhou, S. Ruan, Template-free synthesis of Cu_2O-Co_3O_4 core-shell composites and their application in gas sensing, RSC Adv. 4 (2014) 24211–24216.
[30] Q. Yu, J. Zhu, Z. Xu, X. Huang, Facile synthesis of alpha-Fe_2O_3@SnO_2 core-shell heterostructure nanotubes for high performance gas sensors, Sens. Actuators B Chem. 213 (2015) 27–34.
[31] P. Sun, X. Zhou, C. Wang, K. Shimanoe, G. Lu, N. Yamazoe, Hollow SnO_2/alpha-

Fe_2O_3 spheres with a double-shell structure for gas sensors, J. Mater. Chem. A Mater. Energy Sustain. 2 (2014) 1302–1308.
[32] J. Jiang, L. Shi, T. Xie, D. Wang, Y. Lin, Study on the gas-sensitive properties for formaldehyde based on SnO_2-ZnO heterostructure in UV excitation, Sens. Actuators B Chem. 254 (2018) 863–871.
[33] H. Huang, H. Gong, C.L. Chow, J. Guo, T.J. White, M.S. Tse, O.K. Tan, Low-temperature growth of SnO_2 nanorod arrays and tunable n-p-n sensing response of a ZnO/SnO_2 heterojunction for exclusive hydrogen sensors, Adv. Funct. Mater. 21 (2011) 2680–2686.
[34] S.-W. Choi, A. Katoch, G.-J. Sun, S.S. Kim, Synthesis and gas sensing performance of ZnO-SnO_2 nanofiber-nanowire stem-branch heterostructure, Sens. Actuators B Chem. 181 (2013) 787–794.
[35] F. Wang, J. Liu, X. Wang, J. Kong, S. Qiu, G. Lu, C. He, Alpha-Fe_2O_3@ZnO heterostructured nanotubes for gas sensing, Mater. Lett. 76 (2012) 159–161.
[36] J. Zhang, X. Liu, L. Wang, T. Yang, X. Guo, S. Wu, S. Wang, S. Zhang, Synthesis and gas sensing properties of alpha-Fe_2O_3@ZnO core-shell nanospindles, Nanotechnology 22 (2011).
[37] A.V. Rajgure, N.L. Tarwal, J.Y. Patil, L.P. Chikhale, R.C. Pawar, C.S. Lee, I.S. Mulla, S.S. Suryavanshi, Gas sensing performance of hydrothermally grown CeO_2-ZnO composites, Ceram. Int. 40 (2014) 5837–5842.
[38] S. Yan, S. Ma, X. Xu, Y. Lu, H. Bian, X. Liang, W. Jin, H. Yang, Synthesis and gas sensing application of porous CeO_2-ZnO hollow fibers using cotton as biotemplates, Mater. Lett. 165 (2016) 9–13.
[39] C. Dong, X. Liu, B. Han, S. Deng, X. Xiao, Y. Wang, Nonaqueous synthesis of Ag-functionalized In_2O_3/ZnO nanocomposites for highly sensitive formaldehyde sensor, Sens. Actuators B Chem. 224 (2016) 193–200.
[40] X. Zou, X. Yan, G. Li, Y. Tian, M. Zhang, L. Liang, Solution combustion synthesis and enhanced gas sensing properties of porous In_2O_3/ZnO heterostructures, RSC Adv. 7 (2017) 34482–34487.
[41] Z. Zhang, M. Xu, L. Liu, X. Ruan, J. Yan, W. Zhao, J. Yun, Y. Wang, S. Qin, T. Zhang, Novel SnO_2@ZnO hierarchical nanostructures for highly sensitive and selective NO_2 gas sensing, Sens. Actuators B Chem. 257 (2018) 714–727.
[42] J. Liu, T. Wang, B. Wang, P. Sun, Q. Yang, X. Liang, H. Song, G. Lu, Highly sensitive and low detection limit of ethanol gas sensor based on hollow ZnO/SnO_2 spheres composite material, Sens. Actuators B Chem. 245 (2017) 551–559.
[43] M. Poloju, N. Jayababu, E. Manikandan, M.V.R. Reddy, Enhancement of the isopropanol gas sensing performance of SnO_2/ZnO core/shell nanocomposites, J. Mater. Chem. C 5 (2017) 2662–2668.
[44] J. Song, E. Zheng, X.-F. Wang, W. Tian, T. Miyasaka, Low-temperature-processed ZnO-SnO_2 nanocomposite for efficient planar perovskite solar cells, Sol. Energy Mater. Sol. Cells 144 (2016) 623–630.
[45] H. Nguyen Khac, D.-Y. Son, I.-H. Jang, C.-R. Lee, N.-G. Park, Hierarchical SnO_2 nanoparticle-ZnO nanorod photoanode for improving transport and life time of photoinjected electrons in dye-sensitized solar cell, ACS Appl. Mater. Interfaces 5 (2013) 1038–1043.
[46] A. Hamrouni, N. Moussa, F. Parrino, A. Di Paola, A. Houas, L. Palmisano, Sol-gel synthesis and photocatalytic activity of ZnO-SnO_2 nanocomposites, J. Mol. Catal. A-Chem. 390 (2014) 133–141.
[47] P. Pascariu, A. Airinei, N. Olaru, L. Olaru, V. Nica, Photocatalytic degradation of Rhodamine B dye using ZnO-SnO_2 electrospun ceramic nanofibers, Ceram. Int. 42 (2016) 6775–6781.
[48] F. Belliard, J.T.S. Irvine, Electrochemical performance of ball-milled ZnO-SnO_2 systems as anodes in lithium-ion battery, J. Power Sources 97 (8) (2001) 219–222.
[49] T. Jia, J. Chen, Z. Deng, F. Fu, J. Zhao, X. Wang, F. Long, Facile synthesis of Zn-doped SnO_2 dendrite-built hierarchical cube-like architectures and their application in lithium storage, Mater. Sci. Eng. B 189 (2014) 32–37.
[50] Q. Xie, Y. Zhao, H. Guo, A. Lu, X. Zhang, L. Wang, M.-S. Chen, D.-L. Peng, Facile preparation of well-dispersed CeO_2-ZnO composite hollow microspheres with enhanced catalytic activity for CO oxidation, ACS Appl. Mater. Interfaces 6 (2014) 421–428.
[51] J.C. Dupin, D. Gonbeau, P. Vinatier, A. Levasseur, Systematic XPS studies of metal oxides, hydroxides and peroxides, Phys. Chem. Chem. Phys. 2 (2000) 1319–1324.
[52] Q. Wei, P. Song, Z. Yang, Q. Wang, Hierarchical assembly of Fe_2O_3 nanorods on SnO_2 nanospheres with enhanced ethanol sensing properties, Physica E 103 (2018) 156–163.
[53] N. Xie, L. Guo, F. Chen, X. Kou, C. Wang, J. Ma, Y. Sun, F. Liu, X. Liang, Y. Gao, X. Yan, G. Lu, Enhanced sensing properties of SnO_2 nanofibers with a novel structure by carbonization, Sens. Actuators B Chem. 271 (2018) 44–53.
[54] H. Zhang, J. Yi, Enhanced ethanol gas sensing performance of ZnO nanoflowers decorated with $LaMnO_3$ perovskite nanoparticles, Mater. Lett. 216 (2018) 196–198.
[55] Z. Yuan, L. Yin, H. Ding, W. Huang, C. Shuai, J. Deng, One-step synthesis of single-crystalline ZnO nanowires for the application of gas sensor, J. Mater. Sci-Mater. Electron. 29 (2018) 11559–11565.
[56] Y. Zhang, Y. Liu, L. Zhou, D. Liu, F. Liu, F. Liu, X. Liang, X. Yan, Y. Gao, G. Lu, The role of Ce doping in enhancing sensing performance of ZnO-based gas sensor by adjusting the proportion of oxygen species, Sens. Actuators B Chem. 273 (2018) 991–998.
[57] H. Gong, C. Zhao, F. Wang, On-chip growth of SnO_2/ZnO core-shell nanosheet arrays for ethanol detection, IEEE Electron Device Lett. 39 (2018) 1065–1068.
[58] Z. Li, Q. Zhao, W. Fan, J. Zhan, Porous SnO_2 nanospheres as sensitive gas sensors for volatile organic compounds detection, Nanoscale 3 (2011) 1646–1652.
[59] H.-C. Chiu, C.-S. Yeh, Hydrothermal synthesis of SnO_2 nanoparticles and their gas-sensing of alcohol, J. Phys. Chem. C 111 (2007) 7256–7259.
[60] X. Chi, C. Liu, L. Liu, Y. Li, Z. Wang, X. Bo, L. Liu, C. Su, Tungsten trioxide nanotubes with high sensitive and selective properties to acetone, Sens. Actuators B Chem. 194 (2014) 33–37.
[61] Z. Wen, L. Tian-mo, Gas-sensing properties of SnO_2-TiO_2-based sensor for volatile organic compound gas and its sensing mechanism, Phys. B-Condens. Matter 405 (2010) 1345–1348.
[62] B. Mondal, B. Basumatari, J. Das, C. Roychaudhury, H. Saha, N. Mukherjee, ZnO-SnO_2 based composite type gas sensor for selective hydrogen sensing, Sens. Actuators B Chem. 194 (2014) 389–396.

Xueli Yang received her B. Eng. degree in 2013 and M.S. degree in 2016 from College of Science, Northeast Forestry University in China. Currently she is studying for her Ph.D. degree in College of Electronic Science and Engineering, Jilin University, China. Her research interests focus on the synthesis and characterization of semiconductor oxide functional materials and gas sensors.

Sufang Zhang received the BS degree in Department of Electronic Science and Engineering in 2017. She is currently studying for her MS degree in College of Electronic Science and Engineering, Jilin University, China. Now, her research interests include the synthesis of functional materials and their applications in gas sensors.

Qi Yu received the BS degree in Department of Electronic Science and Engineering in 2017. Now she is currently studying for her MS degree in College of Electronic Science and Engineering, Jilin University, China. Her research interests include the synthesis of functional materials and their applications in gas sensors.

Liupeng Zhao received the B. Eng. degree in department of electronic sciences and technology, Jilin University, in 2016. At the same year, he entered his MS course in College of Electronic Science. Now, he is studying for his MS degree, majored in the synthesis and characterization of the semiconducting functional materials and gas sensors.

Peng Sun received his PhD degree from College of Electronic Science and Engineering, Jilin University, China in 2014. He was appointed the lecturer in Jilin University in the same year. Now, he is engaged in the synthesis and characterization of the semiconducting functional materials and gas sensors.

Tianshuang Wang received his BS degree from the Electronics Science and Engineering department, Jilin University, China in 2015. Presently, he is a Ph.D student and interested in the synthesis and characterization of the semiconducting functional materials and gas sensors.

Fangmeng Liu received his PhD degree in 2017 from College of Electronic Science and Engineering, Jilin University, China. Now he is a lecturer of Jilin University, China. His current research interests include the application of functional materials and development of solid state electrolyte gas sensor and flexible device.

Xu Yan received his M.S. degree in 2013 from Nanjing Agricultural University. He joined the group of Prof. Xingguang Su at Jilin University and received his Ph.D. degree in June 2017. Since then, he did postdoctoral work with Prof. Geyu Lu. Currently, his research interests mainly focus on the development of the functional nanomaterials for chem/bio sensors.

Yuan Gao received her PhD degree from Department of Analytical Chemistry at Jilin University in 2012. Now she is an associate professor in Jilin University, China. Her current research is focus on the preparation and application of graphene and semiconductor oxide, especial in gas sensor and biosensor.

Xishuang Liang received the B. Eng. degree in Department of Electronic Science and Technology in 2004. He received his Doctor's degree in College of Electronic Science and Engineering at Jilin University in 2009. Now he is an associate professor of Jilin University, China. His current research is solid electrolyte gas sensor.

Sumei Zhang obtained her PhD from Jilin University of China in 2005. Presently, she is working as associate professor in Electronics Science and Engineering department of Jilin University. Her current research interests are nanoscience and gas sensors.

Geyu Lu received the BS degree in electronic sciences in 1985 and the MS degree in 1988 from Jilin University in China and the Dr. Eng. degree in 1998 from Kyushu University in Japan. Now he is a professor of Jilin University, China. His current research interests include the development of chemical sensors and the application of the function materials.